



Published in final edited form as:

Nature. 2009 December 17; 462(7275): 875–879. doi:10.1038/nature08653.

## Growth Landscape Formed by Perception and Import of Glucose in Yeast

Hyun Youk<sup>1</sup> and Alexander van Oudenaarden<sup>1,2,\*</sup>

<sup>1</sup> Department of Physics, Massachusetts Institute of Technology, Cambridge, MA 02139, USA

<sup>2</sup> Department of Biology, Massachusetts Institute of Technology, Cambridge, MA 02139, USA

### Abstract

An important challenge in systems biology is to quantitatively describe microbial growth using a few measurable parameters that capture the essence of this complex phenomenon. Two key events at the cell membrane – extracellular glucose sensing and uptake – initiate the budding yeast's growth on glucose. However, conventional growth models focus almost exclusively on glucose uptake. Here we present results from growth-rate experiments that cannot be explained by focusing on glucose uptake alone. By imposing a glucose uptake rate independent of the sensed extracellular glucose level, we show that despite increasing both the sensed glucose concentration and uptake rate, the cell's growth rate can decrease or even approach zero. We resolve this puzzle by showing that the interaction between glucose perception and import, not their individual actions, determines the central features of growth and characterize this interaction using a quantitative model. Disrupting this interaction by knocking out two key glucose sensors significantly changes the cell's growth rate, yet uptake rates are unchanged. This is due to a decrease in burden that glucose perception places on the cells. Our work shows that glucose perception and import are separate and pivotal modules of yeast growth whose interplay can be precisely tuned and measured.

---

In 1942 Jacques Monod introduced his microbial growth model<sup>1</sup> that prompted quantitative studies of microbial metabolism<sup>2–13</sup>. This motivated a wealth of mathematical models describing the growth of budding yeast *Saccharomyces cerevisiae* on the key carbohydrate glucose<sup>14</sup>. These models mainly focus on the effect of glucose import on the growth rate. But in addition to importing glucose, yeast senses extracellular glucose through several glucose sensors. These two key events at the cell membrane – glucose sensing and import – then trigger many downstream intracellular molecular events (e.g. transcription, metabolic processes, post-transcriptional modifications) that collectively determine the growth rate<sup>15</sup>. Many conventional models overlook this collective effect by ignoring glucose sensing. Growth behaviors that are qualitatively very different from current models' descriptions may arise if glucose sensing and import are properly taken into account. One approach to

---

Users may view, print, copy, download and text and data- mine the content in such documents, for the purposes of academic research, subject always to the full Conditions of use: [http://www.nature.com/authors/editorial\\_policies/license.html#terms](http://www.nature.com/authors/editorial_policies/license.html#terms)

\*To whom correspondence should be addressed: avano@mit.edu.

#### Author contributions

H.Y. performed the experiments. H.Y. and A.v.O. designed experiments, analysed data and wrote the manuscript.

addressing this deficiency is constructing detailed many-parameter models that attempt to explicitly track each of the vast molecular events involved in the yeast's glucose metabolism<sup>8,9</sup>. Such approach has provided detailed information on the flux of thousands of known metabolic reactions and new insights into yeast's growth on glucose. However, such an approach also conflates the effects of glucose sensing and import because it is not yet known how each of the vast molecular events are altered when glucose import rate is varied independently of the level of extracellular glucose sensed by the cell. The enormous number of metabolites and reactions involved makes experimentally determining each molecular change due to glucose sensing and import challenging. Indeed, a persistent challenge in obtaining a quantitative understanding of microbial growth on nutrients has been identifying just the few parameters that are necessary for extracting the central features from this complex cellular process. A phenomenological model that retains just those essential parameters may provide new insights and central design principles<sup>16,17</sup> underlying microbial growth. Motivated by these considerations, we sought to decouple and measure the separate effects of glucose sensing and import on cell growth, then provide a concise phenomenological model that elucidates how the interaction between the two determines the growth rate.

## Dependence of growth rate on glucose level

To measure and separate out the effects of glucose perception and import on growth rate, we first decouple any control that glucose sensing has on glucose import. Such coupling primarily comes from the two glucose sensors (Snf3 & Rgt2)<sup>18</sup> that drive the transcriptional regulation of the six primary hexose transporters (Hxt1-4, 6 & 7)<sup>19–23</sup> which are responsible for glucose import (Supplementary Fig. 1). Our background strain lacks all the major and minor glucose transporter genes (*hxt1-17*, *agt1*, *stl1*, *gal2*)<sup>24</sup>, thus no sensors affect the transcription level of any transporter genes including the *HXTs*. We made five “single-*HXT*” strains by introducing into the background strain only one of the five primary *HXT* genes (excluding *HXT7*) under the control of the inducible promoter *P<sub>TET07</sub>*. Each of these strains contains just one type of *HXT* gene, and its expression level could be controlled by the inducer doxycycline independently of extracellular glucose (Supplementary Fig. 2).

We measured the log-phase growth rate of the single-*HXT* strains in minimal media containing a range of different concentrations of doxycycline and glucose, whose concentrations were held constant during batch growth for each experiment. We found surprising behaviors in every single-*HXT* strain's growth rate (Fig. 1 and Supplementary Fig. 3). Since glucose no longer regulates the transcription of the sole *HXT* gene in our strains in a complicated manner, one would expect that an increase in extracellular glucose concentration would lead to a simple increase in the single-*HXT* strain's glucose uptake rate (when the doxycycline concentration is held constant). A typical conventional model<sup>14</sup> predicts that the growth rate should thus simply rise as the glucose level increases. Yet, depending on the initial glucose level, a further increase in the glucose level either increases or decreases the “Hxt1-only” strain's growth rate (Fig. 1). This is also true for the growth rates of the “Hxt2-only” and “Hxt4-only” strains. Furthermore, despite growing as well as other strains at low glucose levels, the “*HXT3*-only” and “*HXT6*-only” strains even approach

growth arrest for glucose level higher than 0.02% (Fig. 1). Thus, we observed no systematic relationship between glucose level and growth rate. It is noteworthy that the wild-type strain, unlike these single-*HXT*s, simply grows faster when more glucose is present (Fig. 1), a behavior we will consider more closely later.

## Dependence of growth rate on glucose uptake rate

Using our doxycycline inducible expression system, we were able to show that for every single-*HXT* strain at fixed doxycycline level, the glucose uptake rate increased as the glucose level increased (Fig. 2). To measure glucose uptake rates, we fused yEGFP to the inducible *HXT* gene in each of the single-*HXT* strains (Supplementary Fig. 4). Measuring the average single-cell fluorescence in these strains gave us the relative number of Hxt proteins synthesized in these cells (Supplementary Fig. 5). Using the known Michaelis-Menten parameters of the Hxts25,26, we calculated the cell's total glucose uptake rate. We also directly measured the cell's glucose uptake rate. The directly measured and calculated uptake rates were in good agreement (Supplementary Fig. 6): glucose uptake rate increased as the glucose concentration increased (at constant doxycycline concentration) (Fig. 2 and Supplementary Fig. 7). Hence despite a monotonic increase in both glucose uptake rate and extracellular glucose level, single-*HXT* strains at fixed doxycycline concentration can grow significantly faster, or slower, or even approach growth arrest as seen earlier (Fig. 1), effects that no conventional growth model can either quantitatively or qualitatively describe.

## Phenomenological model of growth

Plotting all five single-*HXT* strains' growth rates and uptake rates together resulted in a wide scatter of data points, where each data point is specified by two coordinates: uptake rate and growth rate (Fig. 3a and Supplementary Fig. 8). This plot reveals that uptake rate alone cannot specify the cell's growth rate. Specifying the glucose concentration by color-coding these data points (i.e., each data point now has three coordinates: (uptake rate, extracellular glucose concentration, growth rate)) causes a striking pattern to emerge (Fig. 3b). This analysis reveals that growth rate  $\mu$  is determined by two independent variables: the glucose uptake rate  $r$ , and the extracellular glucose concentration  $g$ . Our full experimental data set of all five single-*HXT* strains over a wide range of glucose and doxycycline concentrations are described by a single equation

$$\mu(r, g) = P(g) \times \ln\left(\frac{r}{r_c}\right) + \mu_c, \quad [1]$$

where  $\mu_c$  and  $r_c$  are constants specifying the point of convergence of the log-linear lines (Fig. 3b), and the function  $P(g)$  describes the slope of the log-linear correlation between  $\mu$  and  $r$  for each value of  $g$ . This equation does not depend on which Hxt the cell uses for glucose uptake. This slope  $P(g)$  increases with increasing  $g$ , and in turn tends to decrease growth rate (when  $r < r_c$ ).  $P(g)$  quantifies the dramatic effect that the extracellular glucose has on growth rate independently of glucose import – the effect of glucose perception. Qualitatively, Eqn. [1] states that an increase in the extracellular glucose concentration may cause two counteracting effects: an increased glucose uptake rate  $r$  (which tends to increase

growth rate), and an increased perception of extracellular glucose (which tends to decrease growth rate). The net result on growth rate (i.e., whether it rises or falls) is decided by the competition between these opposing effects of glucose perception and uptake. Which one of the two effects dominates depends on the actual values of  $g$  and  $r$ , in particular on the product  $P(g)\ln(r/r_c)$  quantifying the interaction between glucose perception and import (Supplementary text).

The “growth landscape” in Fig. 3c, described by Eqn. [1], shows the full set of growth rates possible for a wide range of  $g$  and  $r$ . Because Eqn. [1] does not distinguish between the type and number of Hxts cells use for glucose import, it is applicable to cells with any number of *HXT* genes, including the wild-type, as long as the cells achieve the uptake rate within the range we probed. The shape of this landscape allows for the unusual growth-rate behaviors observed, including the convex shaped growth rate of the “Hxt1-only” strain (orange path, Fig. 3c), the “Hxt6-only” strain’s path towards growth arrest (red path, Fig. 3c) and the wild-type’s hyperbolic growth rate (blue path, Fig. 3c). The wild-type strain is near the peak of this growth landscape yet its uptake rate is not much higher than those achieved by some single-*HXT* strains. The growth landscape shows that some values of  $(g, r)$  cannot sustain growth ( $\mu = 0$ ). Indeed, for every  $g$ , there is a minimum uptake rate a cell needs to have in order for it to have any chance of growing in that particular glucose environment (Supplementary Fig. 9).

## Manipulation of glucose perception by sensors

Whereas the glucose uptake rate depends on the Hxts, glucose perception – captured by  $P(g)$  – should depend on mechanisms the cell uses to measure the level of extracellular glucose. *Snf3* and *Rgt2* are two glucose sensors primarily known for regulating transcription of both major and minor glucose transporter genes<sup>18, 27</sup> (*HXTs*, *GAL2*, *STL1*, *AGT1*). Since such regulation is disabled in our single-*HXT* strains, we could manipulate  $P(g)$  by knocking out these two glucose sensors without affecting the uptake rate  $r$ . We constructed a panel of single-*HXT* strains with these two sensors deleted (Supplementary Fig. 10). The relationship between growth rates and extracellular glucose concentration in these “sensorless” strains is strikingly different from that in strains with the two sensors intact (Fig. 4a and Supplementary Fig. 11). Growth rates now generally increase as the glucose level increases (at constant doxycycline level). Also, without the sensors the “Hxt3-only” and “Hxt6-only” strains no longer approach growth arrest as the glucose level increases. Because we deleted all minor glucose transporter genes and removed the glucose’s control of the sole transporter expression in our single-*HXT* strains, changes in uptake rate were not the reason for the growth rescues we observed. For every combination of glucose and doxycycline concentrations, the uptake rate of the sensorless strains was nearly identical to the uptake rate of their sensor-containing counterparts (Fig. 4b and Supplementary Fig. 12).

In the sensorless strains, growth rate again explicitly depends on glucose concentration but with much reduced sensitivity (Fig. 4c–d). When *Snf3* and *Rgt2* are absent, a cell in 4% glucose acts as if it were in 0.06% glucose with intact sensors. Since the uptake rate remains virtually unchanged in the single-*HXT* strains when *SNF3* and *RGT2* are deleted, this reduced-sensitivity effect is due to a change in the perception function  $P(g)$ , not uptake rate

$r$  (Fig. 4d). The remaining dependence of the cell's growth rate on the glucose concentration even after *Snf3* and *Rgt2* have been deleted suggests that other sensors may contribute to the effect embodied in  $P(g)$ <sup>28,29</sup>. Nonetheless, our experiments show that *Snf3* and *Rgt2* are the key determinants of  $P(g)$  (as quantified in Fig. 4d).

The behavior depicted by Eqn. [1] should apply to the wild-type strain as well, as long as it achieves an uptake rate within the range probed with the single-*HXT* strains used to construct our growth landscape. We measured the wild-type's uptake rate and found that it was below the critical uptake rate  $r_c$  for glucose concentrations smaller than 0.02% (Fig. 3b and Supplementary Fig. 16). For higher [glucose], the uptake rate exceeds  $r_c$ . When the wild-type cell's uptake rate is below  $r_c$ , its growth rate fits with the trend revealed in Fig. 3b. For higher glucose concentration, the effect of perception on the wild-type's growth rate disappears (Fig. 3b). One possible explanation is that as long as the glucose concentration is not too low, the wild-type escapes the seemingly detrimental effect of perception on growth rate by making enough hexose transporters to go beyond  $r_c$ . But for lower glucose level where its uptake is less than  $r_c$ , it properly tunes the interaction between glucose perception and uptake (quantified by the product  $P(g)\ln(r/r_c)$ ) such that its growth rate will increase when the cell perceives more extracellular glucose. Such tuning suggests that the transcriptional regulation of the *HXT* genes by *Snf3* and *Rgt2* is organized such that the wild-type always climbs uphill in the growth landscape (Fig. 3c) as it perceives an increase in the extracellular glucose concentration.

The critical point ( $\mu_c, r_c$ ) may represent a region of phase transition in the cell's growth and metabolism. The cell dramatically increases its ethanol production rate as its uptake rate increases above the critical rate  $r_c$  (Supplementary Fig. 17). This suggests that when its uptake rate is below  $r_c$ , the cell metabolizes glucose largely through respiration, but then switches to a largely fermentative metabolism as the uptake rate exceeds  $r_c$ . A key rate limiting step in fermentation is import of glucose and therefore the cell only redirects its glucose flux from respiration to fermentation when its glucose uptake rate is sufficiently high<sup>30,31</sup>. Our results suggest that this major redistribution of flux occurs around  $r_c$ .

## Discussion

Glucose perception and import are two separable modules that each affects the growth rate. But it is the interaction between the two modules that ultimately determines the cell's growth rate, and that interaction can be both precisely altered and measured. But why would it make sense that yeast grows according to Eqn. [1], which allows for a possible detrimental growth if the interaction between the perception and import modules is not properly tuned? One explanation may be that yeast has no way to directly 'measure' its glucose import rate in real-time. Indeed, there is no known 'flux sensor' that the yeast uses to measure its glucose import rate in real-time and then adjust the production level of Hxts to change the glucose import rate if the yeast senses that the flux is too low. In fact, Hxt expression levels are primarily set by the extracellular glucose concentration<sup>32</sup> (Supplementary Fig. 1). While yeast certainly can measure the extracellular glucose level directly and the intracellular glucose level indirectly (for example, through the catabolite-repressor Mig1 which uses intracellular glucose as its substrate)<sup>33–35</sup>, knowing the two glucose levels is not sufficient

for the yeast to infer what its glucose import rate is. This is because a given steady-state glucose concentration gradient can be maintained by a combination of wide ranges of glucose import rate and intracellular glucose breakdown rate. Since the cell has no direct way to measure the breakdown rate (there is no known ‘rate sensor’ measuring intracellular glucose breakdown), the cell cannot infer what the glucose import rate is in real-time just from the difference between extracellular and intracellular glucose. Given the engineering difficulty of building ‘flux sensors’, the yeast may have solved the problem by evolving glucose sensors such as *Snf3* and *Rgt2* to measure the extracellular glucose level, then anticipate a certain glucose import rate would be achieved, set up intracellular activities to process glucose being imported at the anticipated rate, and make sure that such an import rate is indeed achieved by putting its *HXT* genes under the control of those glucose sensors (Supplementary Fig. 1).

On-going efforts at large-scale modeling of glucose metabolism, gene regulation<sup>36</sup> and cellular signaling must decouple and consider how the cell’s response varies when glucose uptake rate is varied independently of extracellular glucose level. For instance, microarray studies have shown that hundreds of genes involved in ribosomal biogenesis, which are energetically very costly, are up-regulated by many folds as the yeast is subjected to ever increasing levels of glucose<sup>37</sup>. In these studies, as the level of glucose is increased, so does the glucose import rate. These observed large-scale changes are thus due to the conflated effects of glucose perception and import. It would be interesting to measure which of these changes are due to glucose perception and import separately by decoupling the two effects. We hope that our model, as well as the framework used to extract some key principles from the complexity underlying yeast growth, will assist ongoing efforts to rationally engineer<sup>38–40</sup> and understand microbial metabolism at the systems-level<sup>41–48</sup>.

## METHODS SUMMARY

### Growth rate measurements

Growth rates were measured while the cells were in log-phase growth in 5 mL batch cultures at 30 °C using synthetic media supplemented with the desired doxycycline and glucose concentrations. These concentrations remained nearly constant during growth (Supplementary Information). Using a spectrophotometer (Hitachi U-1800), we measured the optical density ( $OD_{600}$ : Absorbance at  $\lambda = 600$  nm) of these batch cultures over time, and extracted the growth rate of the cells.

### Glucose uptake rate measurements and calculations

Glucose uptake rates were determined by measuring the rate of glucose depletion in the growth medium while the cells were in log-phase growth. It can be shown (Supplementary Information) that the glucose uptake rate per population density of cells (in units:  $\text{mM hr}^{-1}$

$OD_{600}^{-1}$ ) is approximately  $r(G_0) \approx \mu \frac{(G_0 - G(t))}{\rho(t) - \rho_0}$ , where  $\rho(t) - \rho_0$  is the measured change in  $OD_{600}$  of the cell culture after time  $t$ ,  $\mu$  is the log-phase growth rate, and  $G_0 - G(t)$  is the depleted glucose concentration in the growth medium after time  $t$ . This depleted glucose concentration was measured using a standard commercial ‘glucose assay kit’ (Sigma G3293)

that is based on the conversion of glucose through hexokinase and NADP<sup>+</sup> dependent glucose-6-phosphate-dehydrogenase. We compared the measured glucose uptake rates with the uptake rates calculated using an independent method for the fluorescent single-*HXT* and wild-type strains. We calculated the glucose uptake rates by using the known Michaelis-Menten parameters ( $V_m$  and  $K_m$ ) of Hxts26 and the relative number of Hxt proteins per cell inferred from measuring the average single-cell yEGFP fluorescence (Supplementary Information). These comparisons showed a close agreement between our measured and calculated uptake rates (Supplementary Figs. 6 & 14).

## METHODS

### Strain background and construction

A list of strains with diagrams summarizing their key features are provided in the supplementary information section. All strains were derived from the haploid strain CEN.PK2-1C (*MAT a*, kind gift from E. Boles)<sup>24</sup>, referred to as the “wild-type” in our study. Both EB.Y.VW4000 and EB.Y.VW5000 are deficient in hexose transport due to deletions of all *HXT* genes as well as genes encoding transporters with minor glucose uptake capabilities (*agt1 ydl247w yjr160*)<sup>24</sup>. HY4D1 and HY5F1 each contain rtTA protein expressed constitutively by the *MYO2* promoter (inserted into EB.Y.VW4000 and EB.Y.VW5000 respectively using plasmid pDH18 (EUROSCARF) containing *HIS5* gene) and CFP constitutively expressed by  $P_{TEF1}$ . *XhoI-P\_{TET07}-BamHI*, *BamHI-HXTn-NotI* fragments were cloned into pRS305 (EUROSCARF) backbone containing *LEU2* gene ( $n=1-4, 6$ ). Integrating these plasmids into defective *LEU2* locus (*leu2-3*) in HY4D1 by linearizing the plasmids with *NarI*, the “single-*HXT*” strains were constructed. To construct fluorescent “single-*HXT*” strains, *yEGFP-T\_{ADHI}-Kan* fragment was amplified from pKT127 plasmid (EUROSCARF) and was fused to C-terminus of *HXTn* ORF in each of the single-*HXT* strains via standard PCR integration<sup>49</sup>. This fragment was also fused to C-terminus of *HXTn* ORF ( $n=1-4, 6, 7$ ) in CEN.PK2-1C, thus resulting in six fluorescent wild-type strains (Supplementary Fig. 16). The “sensorless” versions of single-*HXT* strains (*snf3 rgt2*) were constructed in the same way as their sensor-intact counterparts mentioned above by using HY5F1 instead of HY4D1. To probe the wild-type’s transcriptional regulation of each of the *HXT* genes (Supplementary Fig. 1), *XhoI-P\_{HXTn}-BamHI*, *BamHI-YFP-NotI* fragments were cloned into pRS305 backbone containing *LEU2* gene ( $n=1-4, 7$ ) and was integrated into the defective *LEU2* locus (*leu2-3*) in CEN.PK2-1C by linearizing the plasmid with either *NarI* (for  $n=1$ ) or *Clal* (for all other  $n$ ), resulting in five strains. The  $P_{HXT1}$ ,  $P_{HXT2}$ ,  $P_{HXT3}$ ,  $P_{HXT4}$ , and  $P_{HXT7}$  promoter sequences refer to 1941-, 850-, 1996-, 1544-, 2042-bp upstream of the start codon of the respective genes. These sequences include all the known binding sites of transcription factors for the respective genes<sup>50</sup>.

### Growth rate measurements

All growth rates reported in our study were measured while the cells were in log-phase growth in 5 mL batch cultures at 30 °C, in a standard synthetic media with various combinations of glucose and doxycycline concentrations. To bring the cells into log-phase, the single-*HXT* strains were first grown in a standard synthetic media containing 2% maltose and the desired concentration of doxycycline until the cells have been in log-phase for

roughly 12 hours. This procedure ensured that the cells were already making Hxts needed to initiate glucose uptake immediately after being transferred to glucose media. Then these cells were diluted into the standard synthetic media with the same amount of doxycycline, but this time containing glucose instead of maltose. These dilutions were done such that by the time the density of cells in the batch culture reached level detectable by our spectrophotometer (Hitachi U-1800) (roughly 15 hours after dilution), the cells had adjusted to the glucose media and were in log-phase growth. Hence, the transient growth rate change associated with maltose to glucose media transfer did not enter into our growth rate measurements. In a separate experiment, we confirmed this was indeed the case by further diluting these cultures into an identical glucose media, which showed that having the cells pre-grown in maltose before did not affect the growth rates reported in our study. By measuring the Optical Density (OD<sub>600</sub> : Absorbance at  $\lambda = 600$  nm) of these batch cultures over time, we extracted the growth rate of the cells. Strains that approached growth arrest also went through the same procedure as above. Upon transfer to glucose media from maltose media, these cells' growth rates transiently decreased to nearly zero during a period of roughly 24 hours. By looking at the cells under the microscope, no abnormal cell morphologies were detected, thus indicating normal growth (i.e. no pseudohyphal or filamentous growth was detected).

### Fluorescence measurements

The average single-cell fluorescence due to yEGFP fused to C-terminus of *HXT* genes in both the wild-type and the single-*HXT* strains was measured using a Becton Dickinson FACScan flow cytometer with excitation laser at 488nm. Emission filter FL1 (530/30) was used to detect the yEGFP fluorescence levels as well as the YFP for determining the  $P_{TET07}$  induction curves in the calibration strains HY4DCal5 and HY5FCal2. Before observation using FACscan, the strains were grown using the protocol outlined in "growth rate measurements" section. The mean fluorescence values reported in our study represent the steady-state levels of Hxt proteins in single cells, since no appreciable changes in fluorescence was detected while the cells were growing in log-phase.

### Glucose uptake rate measurements and calculations

Glucose uptake rates of cells were determined by measuring the rate of glucose depletion in the growth medium while the cells were in log-phase growth. First, the reasoning behind this procedure is as follows: If the cell's growth rate at glucose concentration  $G_0$  is  $\mu$ ,  $G(t)$  is the concentration of glucose in the growth medium at time  $t$ ,  $r(G(t))$  is the uptake rate per OD of the cells as a function of extracellular glucose, and  $r$  is the OD of cells at  $t = 0$ , then the decrease in glucose concentration in the growth medium over time  $t$  is

$$G_0 - G(t) = \int_0^t r(G(\tau)) \rho_0 \exp(\mu\tau) d\tau. \quad [2]$$

If this change in glucose concentration is sufficiently small, but large enough to be detectable by our chemical assay (described below), then we can approximate  $r(G(t)) \approx$



$r(G_0)$  and  $\mu$  as a constant during the time interval  $t$ . Then above equation can be solved for  $r(G_0)$ :

$$r(G_0) \approx \mu \frac{(G_0 - G(t))}{\rho(t) - \rho_0}, \quad [3]$$

where  $r(G_0)$  is the uptake rate per OD<sub>600</sub>, measured in units of mM hr<sup>-1</sup> OD<sub>600</sub><sup>-1</sup>. This was then converted into molecules sec<sup>-1</sup> cell<sup>-1</sup> using conversion factor 1.7 × 10<sup>7</sup> cells ml<sup>-1</sup> OD<sub>600</sub><sup>-1</sup>.  $\rho(t) - \rho_0$  is the change in OD<sub>600</sub> of the cells measured using the spectrophotometer (Hitachi U-1800), and  $\mu$  is the growth rate determined by the method mentioned previously. The change in glucose concentration  $G_0 - G(t)$  was measured using the standard commercial glucose assay kit (Sigma G3293) based on conversion of glucose through hexokinase and NADP<sup>+</sup> dependent glucose-6-phosphate-dehydrogenase. We compared the measured glucose uptake rates with the uptake rates calculated using an independent method for the fluorescent single-*HXT* and wild-type strains. We calculated the glucose uptake rates by using the known Michaelis-Menten parameters ( $V_m$  and  $K_m$ ) of Hxts26 and the relative number of Hxt proteins per cell inferred from measuring the average single-cell yEGFP fluorescence (Supplementary Information). These comparisons showed a close agreement between our measured and calculated uptake rates (Supplementary Figs. 6 & 14).

## Supplementary Material

Refer to Web version on PubMed Central for supplementary material.

## Acknowledgments

We thank E. Boles (Goethe Universitat, Frankfurt am Main) for kind gift of strains. We also thank D. Botstein (Princeton), D. Muzzey (MIT), J. Gore (MIT), and S. Rifkin (MIT) for critical reading of our manuscript and useful discussions. This work was funded by a National Institutes of Health (NIH) Director's Pioneer awarded to A.v.O and grants from the US National Institutes of Health (NIH) and National Science Foundation (NSF). H.Y. was supported by the Natural Sciences and Engineering Research Council of Canada's (NSERC) Graduate Fellowship.

## References

1. Monod, J. Recherches sur la croissance des cultures bacteriennes. Hermann et Cie; 1942.
2. Bennet MR, et al. Metabolic gene regulation in a dynamically changing environment. *Nature*. 2008; 454:1119–1122. [PubMed: 18668041]
3. Zaslaver A, et al. Just-in-time transcription program in metabolic pathways. *Nature Genetics*. 2004; 36:486–491. [PubMed: 15107854]
4. Airoidi E, et al. Predicting cellular growth from gene expression signatures. *PLoS Comp Biol*. 2009; 5:e1000257.
5. Dekel E, Alon U. Optimality and evolutionary tuning of the expression level of a protein. *Nature*. 2005; 436:588–592. [PubMed: 16049495]
6. Krishna S, Semssey S, Sneppen K. Combinatorics of feedback in cellular uptake and metabolism of small molecules. *Proc Natl Acad Sci USA*. 2007; 104:20815–20819. [PubMed: 18093927]
7. Ihmels J, Levy R, Barkai N. Principles of transcriptional control in the metabolic network of *Saccharomyces cerevisiae*. *Nature Biotechnology*. 2003; 22:86–92.
8. Famili I, Forster J, Nielsen J, Palsson BO. *Saccharomyces cerevisiae* phenotypes can be predicted by using constraint-based analysis of a genome-scale reconstructed metabolic network. *Proc Natl Acad Sci USA*. 2003; 100:13134–13139. [PubMed: 14578455]

9. Bilu Y, Shlomi T, Barkai N, Ruppin E. Conservation of expression and sequence of metabolic genes is reflected by activity across metabolic states. *PLoS Comp Biol*. 2:e106.
10. Levine E, Hwa T. Stochastic fluctuations in metabolic pathways. *Proc Natl Acad Sci USA*. 2007; 104:9224–9229. [PubMed: 17517669]
11. Fell, DA. Understanding the control of metabolism. Portland, London: 1997.
12. Savageau, MA. Biochemical systems analysis: A study of function and design in molecular biology. Addison-Wesely; Reading, MA: 1976.
13. Goyal S, Wingreen NS. Growth-induced instability in metabolic networks. *Phys Rev Lett*. 2007; 98(138105):1–4.
14. Nielsen, J.; Villadsen, J.; Liden, G. Bioreaction Engineering Principles. Springer; 2003. p. 235-311.
15. Dickinson, JR.; Schweizer, M. The Metabolism and Molecular Physiology of *Saccharomyces cerevisiae*. CRC; 2004.
16. Alon U. Simplicity in biology. *Nature*. 2007; 446:497. [PubMed: 17392770]
17. Mallavarapu A, Thomson M, Ullian B, Gunawardena J. Programming with models: modularity and abstraction provide powerful capabilities for systems biology. *J R Soc Interface*. 2009; 6:257–270. [PubMed: 18647734]
18. Moriya H, Johnston M. Glucose sensing and signaling in *Saccharomyces cerevisiae* through the Rgt2 glucose sensor and casein kinase I. *Proc Natl Acad Sci USA*. 2004; 101:1572–1577. [PubMed: 14755054]
19. Boles E, Hollenberg CP. The molecular genetics of hexose transport in yeasts. *FEMS Microbiol Rev*. 1997; 21:85–111. [PubMed: 9299703]
20. Reifengerger E, Freidel K, Ciriacy M. Identification of novel *HXT* genes in *Saccharomyces cerevisiae* reveals the impact of individual hexose transporters on glycolytic flux. *Mol Microbiol*. 1995; 16:157–167. [PubMed: 7651133]
21. Bisson LF, Coons DM, Kruckeberg AL, Lewis DA. Yeast sugar transporters. *Crit Rev Biochem Mol Biol*. 1993; 28:259–308. [PubMed: 8403984]
22. Ozcan S, Johnston M. Three different regulatory mechanisms enable yeast hexose transporter (*HXT*) genes to be induced by different levels of glucose. *Microbiol Mol Biol Rev*. 1999; 63:554–569. [PubMed: 10477308]
23. Pao SS, Paulsen IT, Saier MH Jr. Major facilitator superfamily. *Microbiol Mol Biol Rev*. 1998; 62:1–34. [PubMed: 9529885]
24. Wiczorke R, et al. Concurrent knock-out of at least 20 transporter genes is required to block uptake of hexoses in *Saccharomyces cerevisiae*. *FEBS Lett*. 1999; 464:123–128. [PubMed: 10618490]
25. Reifengerger E, Boles E, Ciriacy M. Kinetic characterization of individual hexose transporters of *Saccharomyces cerevisiae* reveals the impact of individual hexose transporters on glycolytic flux. *Eur J Biochem*. 1997; 245:324–333. [PubMed: 9151960]
26. Maier A, Volker B, Boles E, Fuhrmann GF. Characterisation of glucose transport in *Saccharomyces cerevisiae* with plasma membrane vesicles (countertransport) and intact cells (initial uptake) with single Hxt1, Hxt2, Hxt3, Hxt4, Hxt6, Hxt7 or Gal2 transporters. *FEMS Yeast Res*. 2002; 2:539–550. [PubMed: 12702270]
27. Walsh MC, Scholte M, Valkier J, Smits HP, van Dam K. Glucose sensing and signaling properties in *Saccharomyces cerevisiae* require the presence of at least two members of the glucose transporter family. *J Bacteriol*. 1996; 170:2593–2597. [PubMed: 8626327]
28. Jiang Y, Davis C, Broach J. Efficient transition to growth on fermentable carbon sources in *Saccharomyces cerevisiae* requires signaling through the Ras pathway. *EMBO J*. 1998; 17:6942–6951. [PubMed: 9843500]
29. Boer VM, Amini S, Botstein D. Influence of genotype and nutrition on survival and metabolism of starving yeast. *Proc Natl Acad Sci USA*. 2008; 105:6930–6935. [PubMed: 18456835]
30. van Hoek P, van Dijken J, Pronk J. Effects of specific growth rate on fermentative capacity of baker's yeast. *App Env Microbiol*. 1998; 64:4226–4233.

31. Reijenga KA, et al. Control of glycolytic dynamics by hexose transport in *Saccharomyces cerevisiae*. *Biophys J*. 2001; 80:626–634. [PubMed: 11159431]
32. Kaniak A, Xue Z, Macool D, Kim JH, Johnston M. Regulatory network connecting two glucose signal transduction pathways in *Saccharomyces cerevisiae*. *Eukaryotic Cell*. 2004; 3:221–231. [PubMed: 14871952]
33. Gancedo JM. The early steps of glucose signaling in yeast. *FEMS Microbio Rev*. 2008; 32:673–704.
34. Kim JH, Johnston M. Two glucose-sensing pathways converge on Rgt1 to regulate expression of glucose transporter genes in *Saccharomyces cerevisiae*. *J Biol Chem*. 2006; 281:26144–26149. [PubMed: 16844691]
35. Santangelo GM. Glucose signaling in *Saccharomyces cerevisiae*. *Micro Mol Biol Rev*. 2006; 70:253–282.
36. Levy S, et al. Strategy of transcription regulation in the budding yeast. *PLoS One*. 2007; 2(e250): 1–10.
37. Yin Z, et al. Glucose triggers different global responses in yeast, depending on the strength of the signal, and transiently stabilizes ribosomal protein mRNAs. *Mol Microbiol*. 2003; 48:713–724. [PubMed: 12694616]
38. Stephanopoulos G. Challenges in engineering microbes for biofuels production. *Science*. 2007; 315:801. [PubMed: 17289987]
39. Lorenz DR, Cantor CR, Collins JJ. A network biology approach to aging in yeast. *Proc Natl Acad Sci USA*. 2009; 106:1145–1150. [PubMed: 19164565]
40. Ostergaard S, Olsson L, Nielsen J. Metabolic engineering of *Saccharomyces cerevisiae*. *Micro Mol Bio Rev*. 2000; 64:34–50.
41. Kell DB. Metabolomics and systems biology: making sense of the soup. *Curr Opin Microbiol*. 2004; 7:296–307. [PubMed: 15196499]
42. Savageau MA, Coelho P, Fasani R, Tolla D, Salvador A. Phenotypes and tolerances in the design space of biochemical systems. *Proc Natl Acad Sci USA*. 2009; 106:6435–6440. [PubMed: 19279208]
43. Ihmels J, et al. Rewiring of the yeast transcriptional network through the evolution of motif usage. *Science*. 2005; 309:938–940. [PubMed: 16081737]
44. Klumpp S, Hwa T. Growth-rate-dependent partitioning of RNA polymerases in bacteria. *Proc Natl Acad Sci USA*. 2008; 105:20245–20250. [PubMed: 19073937]
45. Duarte NC, Palsson BO, Fu P. Integrated analysis of metabolic phenotypes in *Saccharomyces cerevisiae*. *BMC Genomics*. 2004; 5:1471–2164.
46. Daran-Lapujade P, et al. The fluxes through glycolytic enzymes in *Saccharomyces cerevisiae* are predominantly regulated at posttranscriptional levels. *Proc Natl Acad Sci USA*. 2007; 104:15753–15758. [PubMed: 17898166]
47. Castrillo JI, et al. Growth control of the eukaryote cell: a systems biology study in yeast. *J Biol*. 2007; 6:4, 1–25. [PubMed: 17439666]
48. Stelling J. Mathematical models in microbial systems biology. *Curr Opin Microbiol*. 2004; 7:513–518. [PubMed: 15451507]
49. Sheff M, Thorn K. Optimized cassettes for fluorescent protein tagging in *Saccharomyces cerevisiae*. *Yeast*. 2004; 21:661–670. [PubMed: 15197731]
50. Kim JH, Polish J, Johnston M. Specificity and regulation of DNA binding by the yeast glucose transporter gene repressor Rgt1. *Mol Cell Biol*. 2003; 23:5208–5216. [PubMed: 12861007]

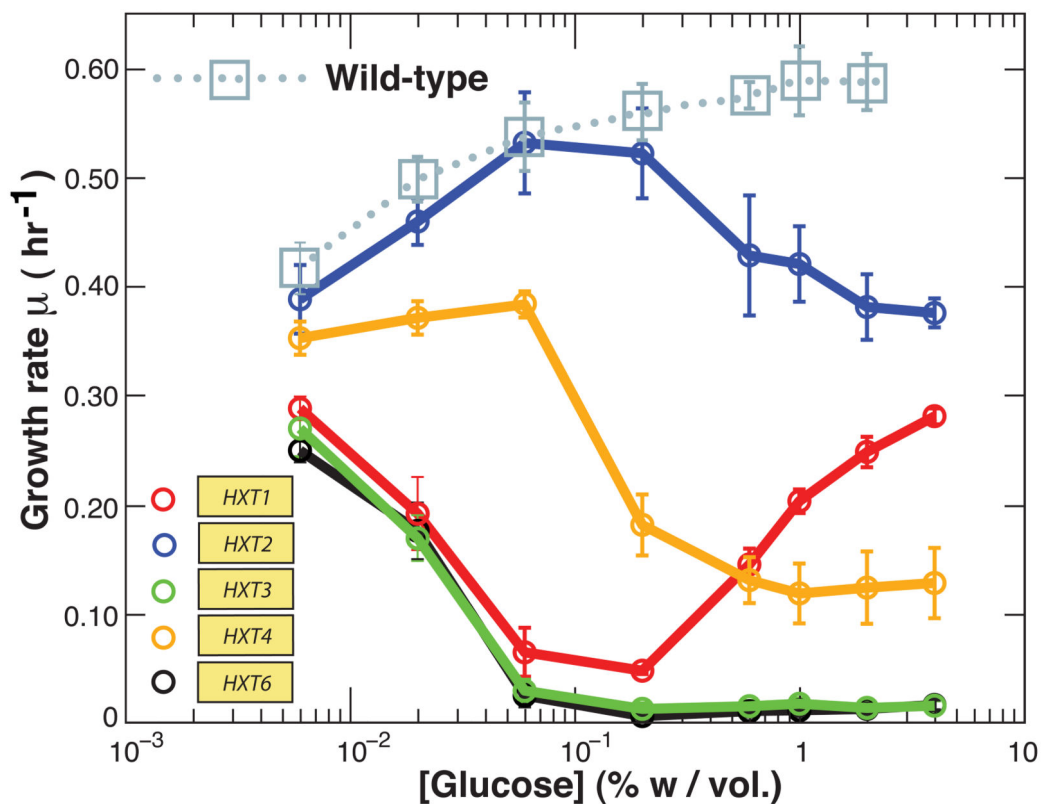


**Figure 1. Growth rates of “single-*HXT*” strains do not show any systematic trend with respect to glucose concentration**

Log-phase growth rates of the wild-type strain (CEN.PK2-1C) and five single-*HXT* strains at varying [glucose] but constant [doxycycline] (0  $\mu\text{g/ml}$  for wild-type and 2.5  $\mu\text{g/ml}$  for single-*HXT* strains) are shown. The shape of each single-*HXT* strain’s growth-rate curve is maintained over a wide range of doxycycline concentrations (Supplementary Fig. 3). The growth-rate curves of the “single-*HXT*” strains display stark differences from the wild-type’s curve: single-*HXT* strains’ growth rates can substantially decrease, and some strains even approach growth arrest, despite a monotonic increase in [glucose]. Error bars, s.e.m.;  $n=3$ .

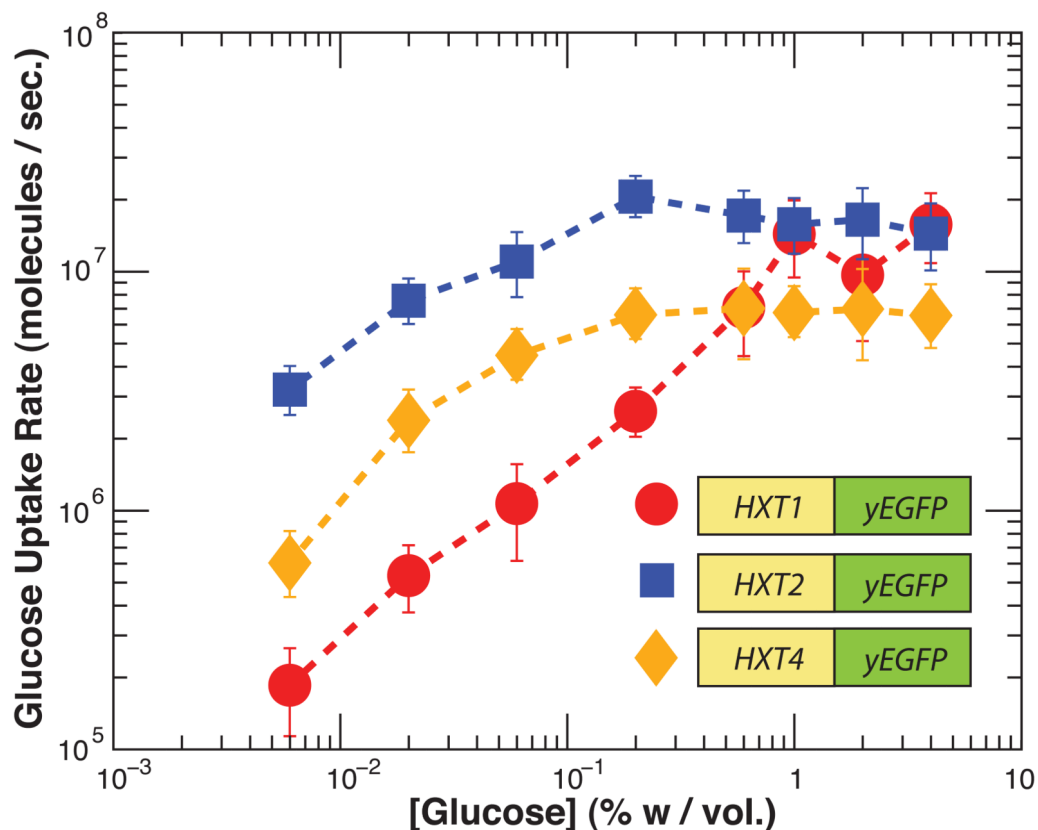


**Figure 2. A rise in [glucose] yields an increase in the uptake rate, but cells do not necessarily grow faster**

To both measure and calculate glucose uptake rates, yEGFP was fused to the *HXT* gene in each “single-*HXT*” strain. These fluorescent single-*HXT* strains have the same growth-rate features as their non-fluorescent counterparts shown in Fig. 1 (Supplementary Fig. 4). The measured glucose uptake rates per cell for just three of these fluorescent single-*HXT* strains at [doxycycline] = 2.5  $\mu\text{g/ml}$  are shown here. These fluorescent single-*HXT* strains’ glucose uptake rates monotonically increase as [glucose] increases, despite the non-systematic behavior of their growth rates reflected in Fig. 1. Hence, a cell can grow faster, or slower, or approach growth arrest despite an increase in both its glucose uptake rate and [glucose]. Error bars, s.e.m.;  $n=3$ .

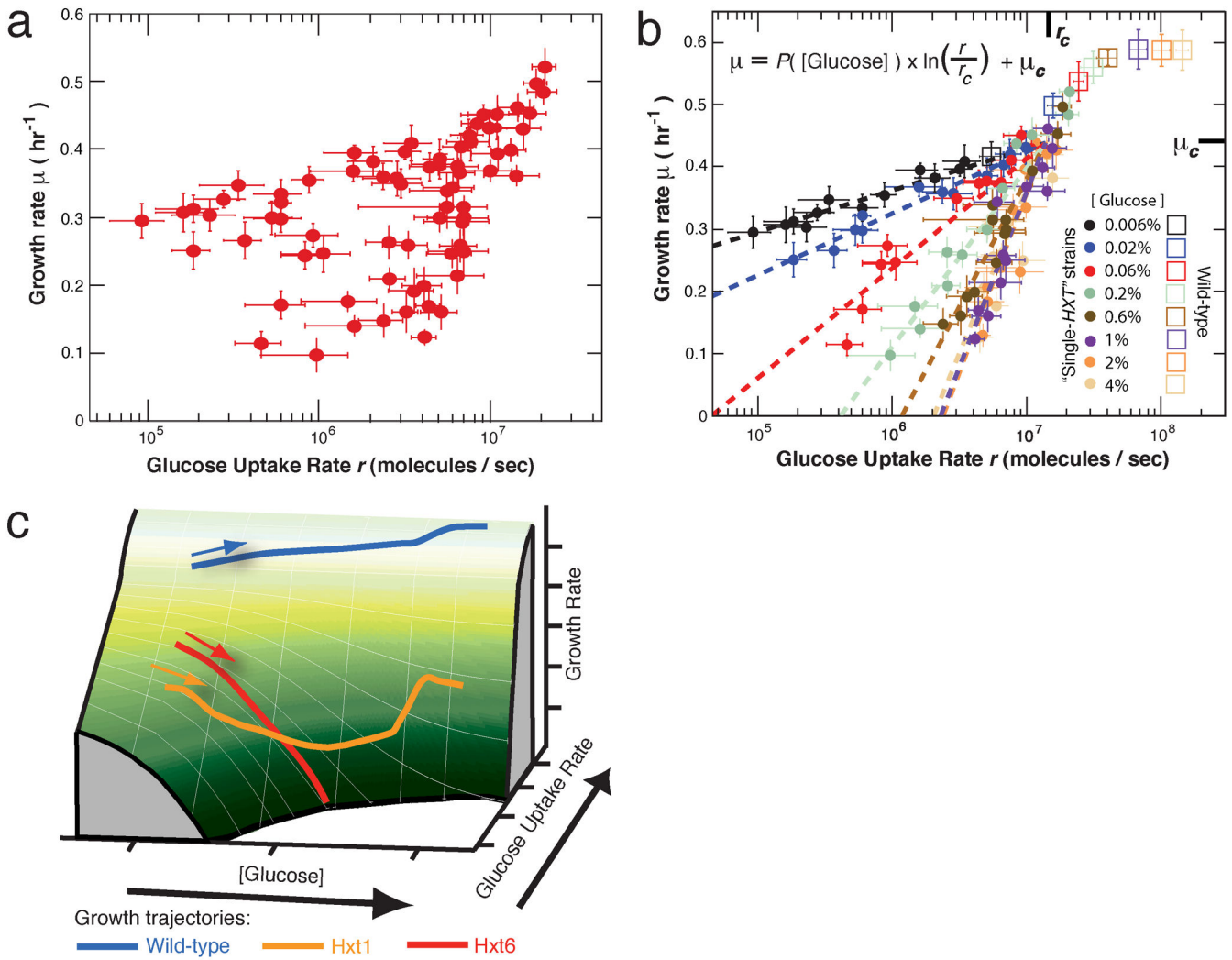


**Figure 3. Emergence of a concise growth model incorporating cell’s perception and uptake rate of glucose, and the resulting “growth landscape”**

**a, b,** Plotting together all the measured growth rates and glucose uptake rates of the fluorescent single-*HXT* strains (a) then color-coding by extracellular glucose level reveals this striking pattern (b). This plot shows that extracellular glucose concentration  $g$  and glucose uptake rate  $r$  are two independent variables. Growth rate is concisely described by the fit function  $\mu(r, g)$ .  $P(g)$  is the slope of the log-linear correlation between growth rate and uptake rate for each  $g$ ; we obtain  $P(g)$  by fitting.  $\mu_c$  and  $r_c$  are constants specifying the point of convergence of the log-linear lines ( $\mu_c = 0.44 \text{ hr}^{-1}$ ,  $r_c = 1.4 \times 10^7$  molecules/s). Error bars, s.e.m.;  $n=3$ . **c,** Full “growth landscape” of budding yeast: Three dimensional plot of the function  $\mu(r, g)$ . The “growth trajectories” followed by the parental wild-type (blue path, near the peak of this landscape), and fluorescent “Hxt1-only” and “Hxt6-only” strains (orange and red paths respectively) are shown. Colored arrows indicate the direction the cell travels on each path as  $g$  increases. The arrows along the two axes (along “[glucose]” and “Glucose uptake rate”) point in the direction of increase.

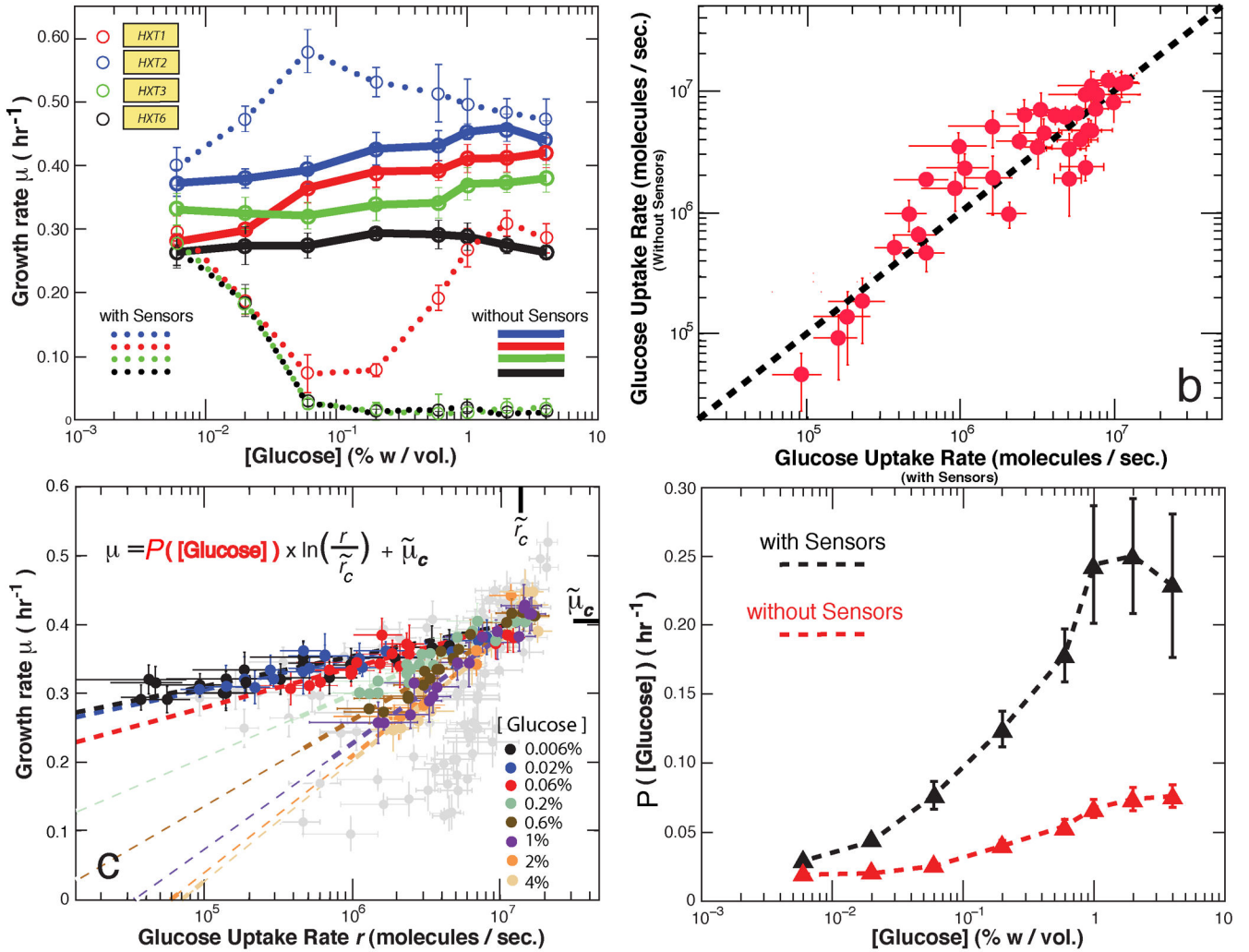


**Figure 4. Manipulation of the cell's perception of extracellular glucose, leaving uptake rate unperturbed, can yield significant growth-rate changes**  
**a,** Growth rates of single-*HXT* strains lacking two glucose sensors (*snf3 rgt2*, bold lines) along with their counterparts with intact sensors (dotted lines) are shown for [doxycycline] = 5  $\mu\text{g/ml}$ . Error bars, s.e.m.; n=3. **b,** Knocking out the two glucose sensors leaves the cell's glucose uptake rate virtually unperturbed. Just the "Hxt1-only" and "Hxt2-only" strains are shown here for simplicity (See Supplementary Figs. 7 & 12 for others). Each data point represents a particular combination of glucose and doxycycline concentrations. Error bars, s.e.m.; n=3. **c,** By yEGFP fusion, fluorescent sensor-less single-*HXT* strains were constructed for comparison with their sensor-intact counterparts. The features of growth rates seen in (a) were preserved after this fusion (Supplementary Figs. 11). Growth rates and glucose uptake rates of these strains were measured (Supplementary Figs. 12–15). For comparison, data for the sensor-intact single-*HXT* strains (from Fig. 3a) are shown in grey ( $\tilde{\mu}_c=0.40 \text{ hr}^{-1}$ ,  $\tilde{r}_c=1.4 \times 10^7 \text{ molecules/s}$ ). Error bars, s.e.m.; n=3. **d,** The sensitivity function  $P(g)$ , calculated from fitting the data in Fig. 3a and 4c is shown for strains with intact

sensors (black) and *snf3 rgt2* strains (red). Error bars indicate 95% confidence interval in these fits.

Author Manuscript

Author Manuscript

Author Manuscript

Author Manuscript